LAWRENCE
LIVERMORE
NATIONAL
LABORATORY

LLNL-JRNL-496611

# An apparatus for the characterization of warm, dense deuterium with inelastic x-ray scattering

P. Davis, G. Collins, T. Doeppner, S. H. Glenzer, R. W. Falcone, J. R. Rygg, W. Unites

August 30, 2011

Journal of Instrumentation

## Disclaimer

Preprint typeset in JINST style - HYPER VERSION

# An apparatus for the characterization of warm, dense deuterium with inelastic x-ray scattering

**P. Davis[a]*, G. Collins[b], T. Doeppner[b], S. Glenzer[b], R. Falcone[a], J. R. Rygg[b] and W. Unites[b]**

[a] *University of California Berkeley, Berkeley, CA 94709, USA*
[b] *Lawrence Livermore National Laboratory, P.O. Box 808, Livermore, CA 94551, USA*
*E-mail:* pfdavis@berkeley.edu

ABSTRACT: We present an instrument platform for studying shock-compressed deuterium on moderately sized laser facilities. Cryogenic liquid deuterium is compressed with a shock driven by a sub-kJ laser pulse. The x-ray probe is the narrow band 2005 eV Si Ly-$\alpha$ resonance produced by a 200 J laser incident on a $Si_3N_4$ foil. Scattered x-ray collection occurs in the backward and forward directions; spectral dispersion with Bragg crystals yields the plasma conditions of density and temperature. Additionally, the shock is probed with velocity interferometry. Combined with the electron density measurements from forward scattering, this allows average ionization state to be inferred. Proof of principle experiments demonstrate the viability of this technique for studies of the ionization of deuterium along the Hugoniot.

KEYWORDS: Keyword1; Keyword2; Keyword3.

*Corresponding author.

## Contents



## 1. Introduction

Spectrally resolved x-ray scattering, or x-ray Thomson scattering (XRTS), has recently been demonstrated to be a powerful diagnostic in the study of warm, dense matter [1]. Of particular interest for planetary science and inertial fusion applications are the properties of dense hydrogenic systems [2]. X-ray scattering provides a method of directly characterizing the plasma conditions of dynamically compressed targets; paired with traditional diagnostic techniques like velocity interferometry, it provides a powerful new method of determining average ionization state as metallization occurs along the shock Hugoniot. In this paper we present an apparatus fielded on a medium-size laser facility capable of characterizing deuterium using x-ray scattering. In particular, we show this platform has the sensitivity and resolution to observe plasmon resonances from the low free electron densities present as ionization begins during compression.

### 1.1 The XRTS diagnostic

A typical XRTS experiment uses high-brightness, narrow-band x-ray emission as a probe; scattered radiation is collected and spectrally dispersed using a Bragg crystal. By varying the scattering angle $\theta$, the scattered wavevector $|k| = 4\pi\frac{E_0}{hc}\sin\frac{\theta}{2}$ can be changed to probe excitations on various scale lengths in the plasma, characterized by the plasma parameter $\alpha = \frac{1}{k\lambda_s} \sim n_e^{1/6}/E_0$ in a Fermi degenerate system. Here, $\lambda_s$ is the screening length and $k$ is the scattering wavevector. In the non-collective regime (backscattering geometry), $\alpha$<1 and inelastic scattering shows the Compton down-shifted line. This spectrum gives the electron velocity distribution function. For collective scattering (forward geometry), $\alpha$>1 and the inelastic feature reveals the plasmon (electron-electron) oscillations.

The study of deuterium using laser-driven shocks has received growing attention because high laser intensities allow very high pressures to be reached dynamically. This has led to detailed measurements of the $D_2$ equation of state at high compression, and the observation of the insulator-metal transition [2]. These studies have used velocity interferometry and radiography to determine shock and particle velocity, thereby constraining thermodynamic variables through the Hugoniot relations.

In contrast to these macroscopic techniques, x-ray Thomson scattering probes microscopic electronic behavior directly. The scattering cross section is a function of the structure factor given by [1],

$$S_{ee}(k,\omega) = |f_I(k) + q(k)|^2 S_{ii}(k,\omega) + Z_f S^0_{ee}(k,\omega) + Z_b \int d\omega' \tilde{S}_{ce}(k,\omega-\omega') S_S(k,\omega').$$

The first term describes contribution from electrons following ion motion; the second is due to the free electrons not following ion motion; the last term includes inelastic scattering by bound core electrons. The spectral shape of non-collective scattering depends strongly on the temperature-dependent distribution function of the electrons in the system; collective scattering is density dependent through the plasmon Bohm-Gross dispersion relation. In addition, the elastic scattering intensity depends strongly on temperature. Taken together, forward and backward scattering can characterize both the electron density and temperature of the system. By combining these measurements with a determination of mass density using one of the above techniques, the average ionization state can also be determined.

## 2. Target Design

### 2.1 X-ray source

Accurate measurements using x-ray scattering impose stringent requirements on the backlighter. In particular, for plasmon measurements, probe bandwidths must be $dE/E < 3 \times 10^{-3}$ and have peak to satellite ratios better than 10, particularly on the low energy wing [3]. This is necessary to descriminate elastic and inelastic components and accurately fit the downshifted plasmon feature. In the Compton regime, $dE/E \sim 10^{-2}$ and $E_{Compton} \sim E^2 \sin^2(\theta/2) > E_0 - E_{sat}$ is needed to differentiate between inelastic scattering and satellites located at $E_{sat}$. Previous experiments using long-pulse laser pumped backlighters have employed the Chlorine Ly-$\alpha$ transition at 2.9 keV [4]. However, weakly shocked deuterium has mass densities several times smaller than the solid density targets studied in previous experiments with Chlorine. In order to achieve collective conditions at fractional ionizations, we have developed the 2005 eV Si Ly-$\alpha$ resonance line as our x-ray probe. For the above conditions, scattering angles of 45° and 135° produce scattering parameters of $\alpha = 1.6$ and $\alpha = 0.65$ at 3x compression and average ionization of 0.2. Thus, this 2 keV probe allows electron plasma waves to be observed at the low electron densities characteristic of the early stages of pressure ionization. In addition, we observe fewer low-energy spectral features compared to the Chlorine line, which is advantageous for accurate determination of the inelastic feature.

Experimental design and source shielding is greatly simplified if the x-ray probe foil is transparent to the source radiation, since using the x-rays in transmission lets the foil act as a natural barrier between the emitting plasma and the target, helping to localize the radiation. Pure silicon

crystal has an attenuation length of 1.56 $\mu$m at 2 keV, and is difficult to produce at micron scale thicknesses, making it difficult to use in transmission. Instead, we employ $Si_3N_4$ film, which is commercially available in sub-micron thicknesses. The 1 $\mu$m thick, 500 $\mu$m square film window is mounted in a 3 mm frame of pure silicon.

We characterize the Si Ly-$\alpha$ $2p-1s$ line using a similar approach as in [5], where a frequency doubled pump laser was shown to give optimally efficient x-ray production. In our case, a 1 ns, 527 nm, 150 J laser pulse irradiated the silicon nitride film; by defocusing and using a 300 $\mu$m phase plate, nominal spot sizes between 100 and 500 $\mu$m were produced. A flat, 24mm square, ZYB grade highly oriented pyrolytic graphite (HOPG) (General Ceramics) crystal was used in mosaic focusing mode [6] to spectrally disperse the resulting x-ray emission. The detector was a Fuji BAS-TR025 image plate (IP).

The digitization process for these image plates results in photon intensity given in units of photostimulated luminenscence (PSL), which is calibrated to incident photon energy. We compute the conversion efficiency of laser energy into the Ly-$\alpha$ line as

$$\eta_{Ly-\alpha} = \frac{h \int I(\omega) d\omega}{\psi_{PSL} \Omega_{det} E_{laser}}$$

where the integral covers the spectral width of the probe line, $I(\omega)$ is the intensity profile in the dispersive direction, $h$ is the spatial extent of the signal in the non-dispersive direction, $\psi_{TR}$ is the energy-PSL calibration factor and $E_{laser}$ is the incident laser energy. $\Omega_{det} = \frac{rh}{4\pi d}$ is the solid angle of the detector, where $d$ is the source-crystal distance and $r$, the integrated reflectivity of the HOPG crystal, has been previously characterized [7]. Below 10 keV, TR image plates have approximately linear sensitivity to incident x-ray energy $E$, measured to be $\psi_{TR} = \eta(m\,\mathrm{E} + c)$ where in the relevant energy range, $m$=0.54 mPSL/keV, $c$=0.02 mPSL and $\eta$=1.0 [8]

Measured conversion efficiencies are plotted in Figure 1 along with conversion efficiency measurements previously made using a Chlorine probe. The trend toward lower efficiency at higher intensities is due to burn-through of the $Si_3N_4$ window. At larger spot sizes, x-ray production is enhanced by additional Ly-$\alpha$ emission from the Si window frame. Peak x-ray production into the Ly-$\alpha$ line is about 0.2 %, which is comparable to previous measurements. The bandwidth of the resonance is $2 \times 10^{-3}$; peak-to-satellite ratios are about 11:1. The two most prominent satellites on the low-energy side of the resonance are located 5 and 28 eV below the primary line whereas expected plasmon shifts for this system range between 5 and 20 eV, depending on compression and ionization. At 135 degree backscatter, the Compton shift is 13.3 eV. Thus, this line is well suited as an x-ray Thomson scattering probe for both collective and non-collective measurements.

### 2.2 Deuterium Vessel

The target consists of a 2 mm diameter cylindrical reservoir bored into a copper block. The target block is fixed to a copper arm which is mounted at the top of the experimental target chamber, illustrated in Figure 2. This arm is helium cooled with a flow cryostat and shielded with an Aluminum casing to minimize radiative heating.

The front opening of the target, seen in Figure 3, is sealed with a 40 $\mu$m Al disk coated with 12 $\mu$m of CH. The aluminum pusher couples the laser energy into a shock which propagates into the bulk deuterium, while minimizing x-ray preheat at the laser-target interface. The plastic

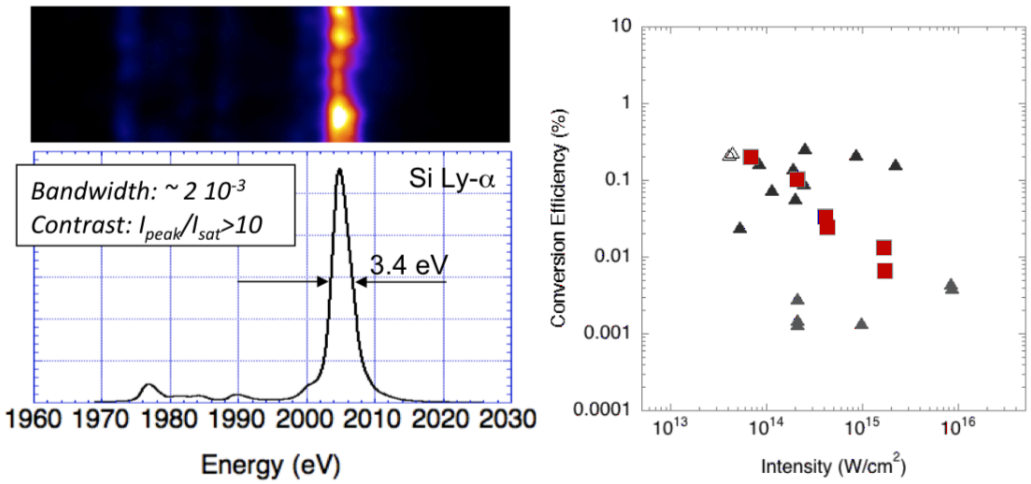


**Figure 1.** Left: Experimental backlighter spectrum and lineout. Right: Conversion efficiency for Si Ly-$\alpha$ (red squares) is plotted with previous measurements of Cl Ly-$\alpha$ at $1\omega$ (light triangles) and $2\omega$ (dark triangles) reported in [5]

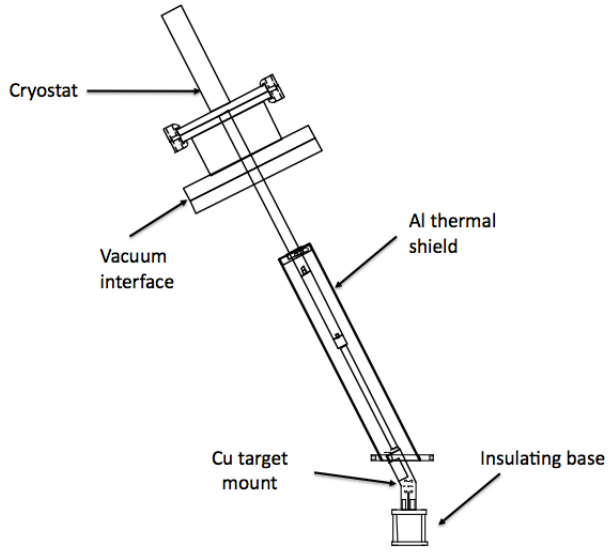


**Figure 2.** Schematic of target mount and cooling assembly.

coating acts as an ablator. The opposite end of the cylinder is sealed with 130 $\mu$m thick quartz; this transparent window allows the VISAR probe to enter the target. It is tilted slightly to avoid unwanted reflections interfering with those from the shock itself. Three 400 $\mu$m holes are bored perpendicular to the cylindrical axis, which is the axis of shock propogation. These act as x-ray entrance and exit windows. They are covered with 3 $\mu$m polypropylene seals to prevent the escape of deuterium. The window in the horizontal plane is additionally coated with a 500 nm layer of

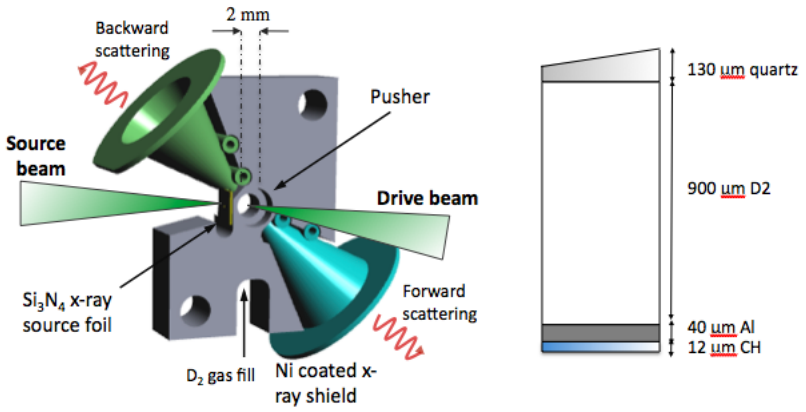


**Figure 3.** Deuterium target, showing backlighter and drive beam positions and x-ray access ports. This target is mounted to the assembly show in Figure 2.

$Si_3N_4$, which acts the x-ray scattering source. The windows at 45° and 135° to the source are apertures for non-collective and collective scattering respectively. By collecting scattered x-rays from both ports as well as VISAR data on a single shot, this platform is designed to provide simultaneous single-shot measurement of density, temperature and shock velocity.

Blow-off plasmas are produced at both the pusher and x-ray source foil. The time-integrated x-ray scattering detectors are shielded from the resulting continuum emission using 250 $\mu$m thick plastic cone shields coated with 50 $\mu$m Ni. The cone and outer lip provide an f-0.8 shield around the scattering window, eliminating direct view of the crystal to continuum x-ray emission.

Deuterium gas is fed into the target through a 500 $\mu$m diameter tube. A Cernox CX-1070 temperature sensor is located in the base of the target mount assembly adjacent to the deuterium cell. This provides an indication of when the phase transition has been reached and also serves as the temperature monitor for the thermal control loop. As the target cools below the liquid transition point, the target reservoir fills with liquid and the remaining gas bubbles out. Since the VISAR diagnostic also provides a real-time view of the target volume through the rear window, this transition can be clearly observed, and confirmed by a rapid drop in pressure. For deuterium, the gas-liquid transition occurs at 19.5K and the liquid-solid transition at 17K at typical backing pressures of 300 bar. A time history of the target cooling cycle is shown in Figure 4, which shows that a temperature gradient of about 7K exists between the cryostat and the target volume at equilibrium. The target is maintained at a temperature above the oxygen melt point until shot time, to minimize ice buildup on the target. Proportional-integral-derivative (PID) control is used to maintain the target at constant thermal conditions prior to a laser shot; gains are tuned to maintain target temperature to within 0.1 K at shot time. A Firerod cartridge heater installed in the base of the target is operated at 5W to provide the necessary temperature source to complete the control loop. Additionally, at higher power settings this heater can be used to heat the target to room temperature after the shot, minimizing condensation during target chamber venting. With this system in place, a two hour shot

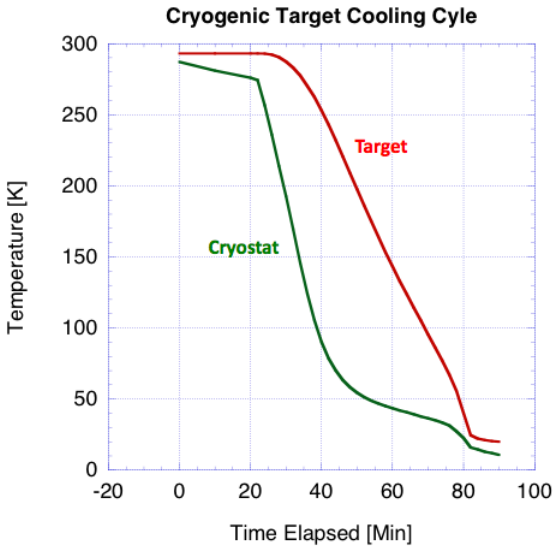


**Figure 4.** Evolution of cryostat and target temperatures during the cooling cycle.

cycle can be achieved.

## 3. Experiment

### 3.1 Layout

The Janus facility at Lawrence Livermore National Laboratory is a 2 beam, Nd:Glass kJ-class laser system. Proof-of-principle experiments were performed there using the target chamber layout shown in Figure 5. In these experiments, the x-ray scattering platform was tested using a 230 J, 2 ns frequency-doubled 527 nm laser pulse incident on a $Si_3N_4$ foil. The beam was defocused to a 400 $\mu$m spot size, resulting in an intensity of $1 \times 10^{14}$ W/cm$^2$ and producing about $10^{15}$ 2 keV photons at the foil.

The target was cooled past the liquid transition to 19K. X-rays were elastically scattered from the liquid at 45° in the forward direction and spectrally dispersed with a high efficiency Bragg crystal. In order to maximize the low-intensity scattering signal, a HOPG crystal was used, curved in the non-dispersive direction with an ROC of 107 mm. The crystal was placed at the Bragg angle $\theta_B$, satisfying $n\lambda = 2d\sin\theta_B$; for the [002] plane of HOPG $2d = 0.67$ nm, so $\theta_B = 67.5°$ at 2 keV. Focusing was acheived by setting the source-crystal and crystal-detector distances to $F = R/\sin\theta_B = 11.6$ cm.

The velocity interferometry diagnostic was tested by launching a shock with a second 2 ns pulse, 230 J, 527 nm pulse focused with a 600 $\mu$m phase plate. This $\sim 4 \times 10^{13}$ W/cm$^2$ drive laser was incident on the pusher, as seen in Figure 5, launching a shock along the axis of the target, which was probed through the rear window with a second 0.5 J, 20 ns, 532 nm beam. The reflected signal from the metallized shock front was sent to a pair of intereferometers coupled to

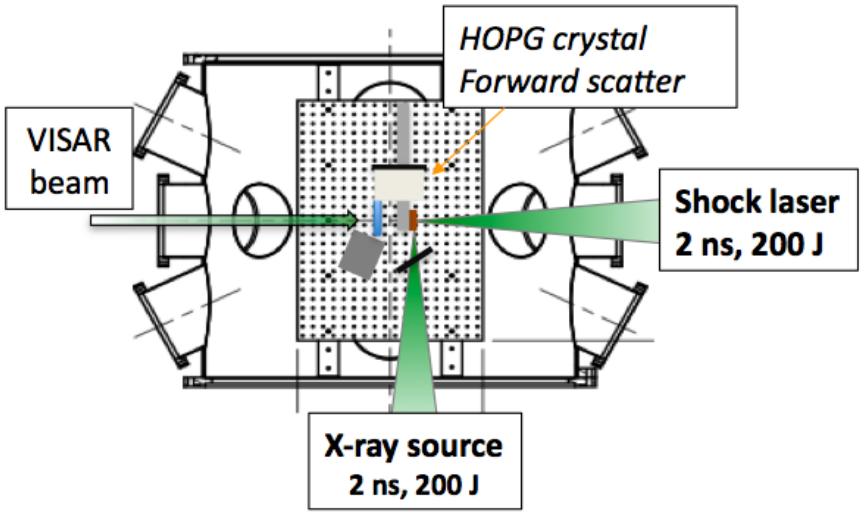


**Figure 5.** Layout of target chamber for preliminary experiments.

optical streak cameras, providing a time history of the shock velocity encoded as a phase shift in the interferogram. The double-interferometer architecture allowed the diagnostic to operate at two sensitivities, resolving the $2\pi$ degeneracy in the fringe shift at the shock front without reducing the precision of the measurement [9].

### 3.2 Results

The performance of the x-ray scattering diagnostic was tested by observing elastic scattering from an unshocked liquid sample. The measured signal is shown in Figure 6. This raw scattering signal shows a continuum background level of about 0.15 PSL with RMS noise of 0.03 PSL, largely due to leakage of undiffracted radiation. The intensity of the elastically scattered signal registers as 0.14 PSL, providing a clearly detectable and easily fit feature.

The throughput of the scattering diagnostic is confirmed by comparing the light in this scattered feature with the measured incident x-rays produced at the source foil. Assuming liquid density and a roughly 600 $\mu$m deep shock front, we expect a scattering fraction of approximately $n_e \sigma_{Thomson} x = 5 \times 10^{-3}$, where $x$ is the scale length over which scattering occurs. Accounting for the composite detector solid angle and integrated crystal reflectivity $\Omega_D = 1 \times 10^{-5}$ and a source-target solid angle of $\Omega_S = 0.03$ this translates into an expected signal of $3 \times 10^4$ photons, or about 0.16 PSL. Repeating the scattering shot with an empty cell shows only continuum noise, confirming that we do not detect stray light scattered from the target itself.

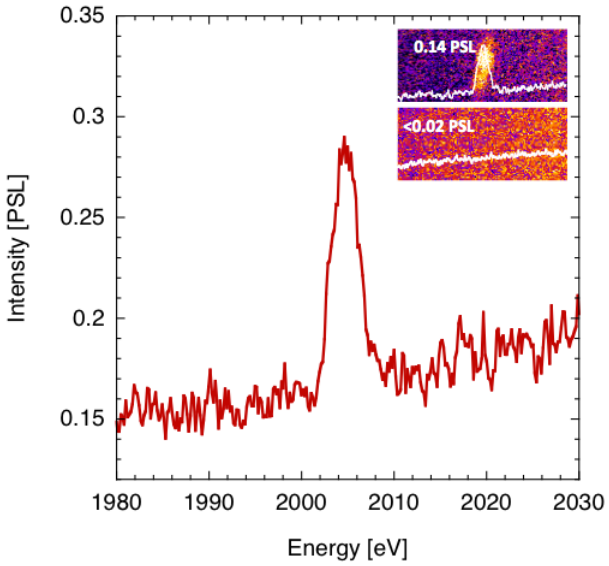


**Figure 6.** Measured 2005 eV x-rays forward scattered from cryogenic liquid deuterium. Instrument resolution is less than 4 eV, and throughput is sufficient for accurate inelastic scattering measurements. Scattering from an identical empty target shows not spurious scattering (inset).

The spectral resolution of the forward scattering spectrometer and source line is measured to be a gaussian profile of 3.8 eV. This is sufficiently high to allow precise measurements of plasmon positions at even low ionization fractions of 0.1 in weakly compressed hydrogen. In Figure 7, we illustrate this with synthetic scattering spectra for ionization states of $Z = 0.1, 0.2$ and 0.5 assuming a mass density of $\rho = 0.5$ g/cm$^3$ and a temperature of $T_e$=0.35 eV. The redshifted inelastic feature from emerging plasmons is already clearly visible as a shoulder on the elastic feature at an ionization of $Z = 0.1$; as ionization increases, the growing electron density causes the plasmon to shift away from the elastic feature to lower energies. The intensity in the plasmon feature also increases with ionization, as more electrons in the system participate in free electron oscillations and therefore are unavailable for elastic scattering. Thus, with the demonstrated spectral resolution, it is possible to track the onset of even small fractional ionizations along the $D_2$ Hugoniot.

To accurately infer ionization, we require establishing the thermodynamic conditions of the plasma at the time it is probed. This is accomplished by measuring shock velocity directly with an optical VISAR diagnostic. The drive beam incident on a 10 $\mu$m CH/40 $\mu$m Al pusher drove a shock sufficiently strong to induce partial metallization and allow a direct velocity measurement. The resulting VISAR trace is shown in Figure 8. The shock releases into the $D_2$ at 23 km/s, decaying to 12 km/s 17 ns later at the end of the streak. These velocities can be mapped to compression and pressure using the $D_2$ equation of state and the single-shot Hugoniot relations. Here, we use recent *ab initio* results [14] to calculate pressure and compression of 18.5 GPa and 3.3x compression at the time the shock enters the view of the XRTS diagnostic.

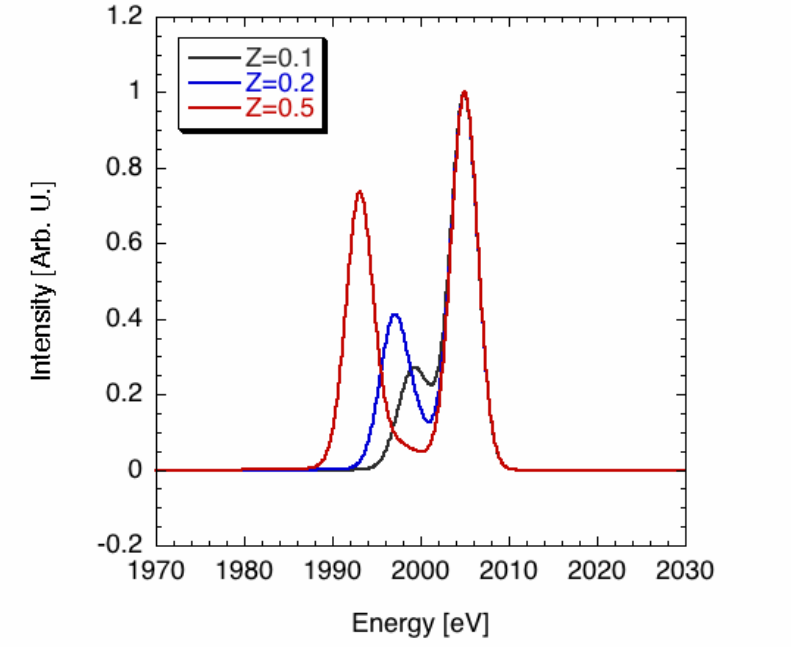


**Figure 7.** Synthetic forward scattering spectra for several fractional ionization states.

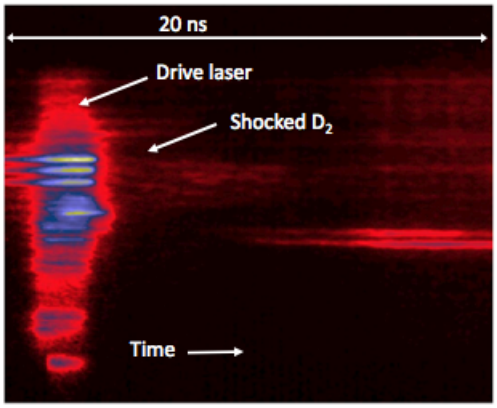


**Figure 8.** Sample VISAR image showing light from the drive beam and decaying shock in $D_2$.

## 4. Conclusion

We have developed an instrument platform capable of investigating the properties of deuterium

under shock conditions using spectrally resolved x-ray scattering. The Si Ly-$\alpha$ resonance is characterized as a viable source for x-ray scattering in systems with electron densities $\sim 1 \times 10^{23}$ cm$^{-3}$. In particular, this probe has the narrow bandwidth and low energy required for collective scattering studies. Preliminary experiments demonstrate that this design is a viable platform for investigating the properties of warm, dense deuterium with moderately sized laser facilities. Future experiments will use this platform as a novel method to investigate deuterium for applications in laser fusion and planetary science.

## Acknowledgments

This work performed under the auspices of the U.S. Department of Energy by Lawrence Livermore National Laboratory under Contract DE-AC52-07NA27344. Supported by LDRD 11-ER-050 and the NNSA SSGF program through the Krell Foundation.

## References

[1] S. Glenzer et al., *X-ray Thomson scattering in high energy density plasmas*, *Rev. Mod. Phys.* **81** (2009)1625.

[2] G. Collins et al., *Measurements of the equation of state of deuterium at the fluid insulator-metal transition*, *Science* **281** (1998) 1178.

[3] O.L. Landen et al., *Dense matter characterization by x-ray Thomson scattering*, *JQSRT* **71** (2001) 465.

[4] S. Glenzer et al., *Observations of plasmons in warm dense matter*, *Phys. Rev. Lett.* **98** (2007) 056002.

[5] M. Urry et al., *JQSRT* **99** (2006) 636.

[6] G. Ice et al., *Mosaic crystal x-ray spectrometer to resolve inelastic background from anomalous scattering experiments*, *Nuc. Inst. & Methods* **A291** (1990) .

[7] A. Pak et al., *X-ray line measurements with high efficiency Bragg crystals*, *Rev. Sci. Inst.* **75** (2004) 3747.

[8] A.L. Meadowcroft et al., *Evaluation of the sensitivity and fading characteristics of an image plate system for x-ray diagnostics*, *Rev. Sci. Inst.* **79** (2008)113102.

[9] P.M. Celliers et al., *Line-imaging velocimeter for shock diagnostics at the OMEGA laser facility*, *Rev. Sci. Inst.* **75** (2004) 4916.

[10] P. Souers., *Hydrogen properties for fusion energy*, University of California, Berkeley 1986.

[11] P. Celliers et al., *Accurate measurement of laser-driven shock trajectories with velocity interferometry*, *Appl. Phys. Lett.* **73** (1998)1320.

[12] G. Gregori et al., *Derivation of the static structure factor in strongly coupled non-equilibrium plasmas for x-ray scattering studies*, *High Energy Density Physics* **3** (2007) 99.

[13] J. MacFarlane et al., *HELIOS-CR - A 1D radiation-magnetohydrodynamics code with inline atomic kinetics modelling*, *JQSRT* **99** (2006) 381.

[14] B. Holst et al., *Thermophysical properties of wam dense hydrogen using quantum molecular dynamics simulations*, *Phys. Rev. B.* **77** (2008) 184201.